Brain Topogr (2017) 30:711–722
DOI 10.1007/s10548-017-0577-8

ORIGINAL PAPER

Minimum-Norm Estimation of Motor Representations in Navigated TMS Mappings

Minna Pitkänen[1,2] · Elisa Kallioniemi[2,3] · Petro Julkunen[2,4] · Maria Nazarova[5] · Jaakko O. Nieminen[1] · Risto J. Ilmoniemi[1]

Received: 27 January 2017 / Accepted: 11 July 2017 / Published online: 18 July 2017

Abstract Navigated transcranial magnetic stimulation (nTMS) can be applied to locate and outline cortical motor representations. This may be important, e.g., when planning neurosurgery or focused nTMS therapy, or when assessing plastic changes during neurorehabilitation. Conventionally, a cortical location is considered to belong to the motor cortex if the maximum electric field (E-field) targeted there evokes a motor-evoked potential in a muscle. However, the cortex is affected by a broad E-field distribution, which tends to broaden estimates of representation areas by stimulating also the neighboring areas in addition to the maximum E-field location. Our aim was to improve the estimation of nTMS-based motor maps by taking into account the E-field distribution of the stimulation pulse. The effect of the E-field distribution was considered by calculating the minimum-norm estimate (MNE) of the motor representation area. We tested the method on simulated data and then applied it to recordings from six healthy volunteers and one stroke patient. We compared the motor representation areas obtained with the MNE method and a previously introduced interpolation method. The MNE hotspots and centers of gravity were close to those obtained with the interpolation method. The areas of the maps, however, depend on the thresholds used for outlining the areas. The MNE method may improve the definition of cortical motor areas, but its accuracy should be validated by comparing the results with maps obtained with direct cortical stimulation of the cortex where the E-field distribution can be better focused.

Keywords Navigated transcranial magnetic stimulation · Minimum-norm estimate · Motor cortex · Motor-evoked potential · Motor representation · Electric field

Introduction

Navigated transcranial magnetic stimulation (nTMS) is considered an accurate and reliable tool for locating functional areas in the cortex; it is already used routinely in presurgical mapping of both motor and language representation areas (Jussen et al. 2016; Paiva et al. 2012; Picht et al. 2011, 2013). TMS has also been used in stroke patients, for example, to predict their clinical outcome (Heald et al. 1993; Jang et al. 2010) and to probe cortical reorganization (Liepert et al. 2000; Traversa et al. 1997). Conventionally, motor maps are obtained by targeting magnetic pulses to different cortical locations while recording motor-evoked potential (MEP) amplitudes and latencies or corticospinal silent-period durations from peripheral muscles (Kallioniemi et al. 2015; Pitkänen et al. 2015; Vitikainen et al. 2013; Wassermann et al. 1993; Wilson et al. 1993). The area thus obtained can be further outlined, for example, by spline-interpolating the MEP amplitudes to a fine

✉ Minna Pitkänen
minna.pitk@gmail.com

1 Department of Neuroscience and Biomedical Engineering, Aalto University School of Science, P. O. Box 12200, FI-00076 Aalto, Espoo, Finland

2 Department of Clinical Neurophysiology, Kuopio University Hospital, P. O. Box 100, FI-70029 Kuopio, Finland

3 Department of Clinical Radiology, Kuopio University Hospital, P. O. Box 100, FI-70029 Kuopio, Finland

4 Department of Applied Physics, University of Eastern Finland, P. O. Box 1627, FI-70211 Kuopio, Finland

5 Centre for Cognition and Decision Making, National Research University Higher School of Economics, 46B Volgogradskiy Prospekt, Moscow, Russian Federation 109316

grid of cortical locations, defining the 50-μV MEP contour line, and including in the area only those locations that lie within this line (Borghetti et al. 2008; Julkunen 2014). The center of the map can be identified by calculating the center of gravity (CoG) (Wassermann et al. 1992). Currently used mapping methods are based on a simplified model of nTMS where only a small cortical point at the electric field (E-field) maximum would be activated. However, due to the extent of the E-field, nTMS can activate also neighboring areas (Opitz et al. 2014; Thickbroom et al. 1998). Therefore, the motor areas deduced from nTMS trials tend to be larger than those obtained with the more focused direct cortical stimulation (DCS) (Vitikainen et al. 2013) and might thus be misleading. If the nTMS-induced E-field distribution is included in the calculations, more accurate estimates of the extent of motor areas could be expected.

The effect of the E-field distribution on the estimation of motor maps has been investigated previously (Bohning et al. 2001; Matthäus et al. 2008; Opitz et al. 2014; Thielscher and Kammer 2002). Bohning et al. (2001) calculated the deconvolution of the TMS-induced E-field distribution in the brain and the measured MEP amplitudes to estimate motor representation areas. Thielscher and Kammer (2002), on the contrary, considered activated voxels to be those in which the E-field strength is most similar for different coil locations from which a similar MEP would result. These studies were conducted with non-navigated TMS. Opitz et al. (2013, 2014) used nTMS and estimated motor areas by weighting the mean E-field distribution by MEP amplitudes, whereas Matthäus et al. (2008) determined the activation areas by computing the correlation between the E-field strength and the evoked responses. E-field calculations have also been combined with hierarchical model fitting to determine likely stimulated targets in a standard visual suppression paradigm (Thielscher and Wichmann 2009). Previous studies have also looked at the different components of the induced E-field, such as those tangential or normal to the cortex, when estimating the site activated by TMS (Bungert et al. 2016; Opitz et al. 2013). Furthermore, conventional nTMS measurements have been improved by exploiting stimulation intensities based on the E-field strength to reduce stimulator-dependent differences in the results (Danner et al. 2008; Julkunen et al. 2012) and by considering the input–output relationship between the MEP amplitudes and stimulation intensities to reduce inter-individual variation in the motor maps (Kallioniemi and Julkunen 2016).

In the present study, motivated by the research of Bohning et al. (2001), we take into account the effect of the spatial pattern of the E-field when determining the nTMS-mapped primary motor areas by applying the minimum-norm estimate (MNE). MNE (Hämäläinen and Ilmoniemi 1994; Parker 1977) is a solution to an inverse problem and is advantageously used to estimate source current distributions in the brain from magnetoencephalogram or electroencephalogram signals in cases when only minimal or no a priori information about the sources is available. Here, the inverse problem is to find the motor representation area based on a number of nTMS–MEP trials. The MNE method is similar to the deconvolution of TMS maps (Bohning et al. 2001). We aim to further improve the method of Bohning et al. by applying nTMS and MNE with regularization in order to increase the accuracy of the TMS maps. We calculate the E-field in a spherical model instead of measuring it in a phantom and apply vectorial approach whereas Bohning et al. utilized only the magnitude of the E-field and assumed that the nerve bends and orientations were randomly distributed. Moreover, we determine motor representation areas with greater resolution and show the results in individual anatomies of the subjects. This work may lead, for example, to better nTMS assessment of cortical reorganization after stroke or other brain damage.

Materials and Methods

MNE gives the simplest (in principle, in the case of a linear response model and the absence of any a priori information about the cortical excitability distribution, the most accurate) excitability maps that can explain TMS-evoked motor responses. Here, the muscle response is approximated to be proportional to a sigmoidal function of the induced E-field on the cortex so that after a certain E-field strength, the response amplitudes start to increase until they reach a plateau (Devanne et al. 1997). Therefore, similarly to a previous study (Bohning et al. 2001), the E-field distribution was transformed with a sigmoidal function to obtain an "activating function" $E'(\mathbf{r})$, i.e., a function that describes how the motor response amplitude depends on the E-field:

$$E'(\mathbf{r}) = M\frac{1+\operatorname{erf}\left(\frac{E(\mathbf{r})-\mu}{\sigma\sqrt{2}}\right)}{2}, \quad (1)$$

where M is the response maximum, $E(\mathbf{r})$ the E-field intensity at location $\mathbf{r}$, erf the error function, with μ and σ defining the midpoint and transition width of the sigmoidal function, respectively (Bohning et al. 2001). The erf function is the cumulative distribution function of the Gaussian distribution.

In the present model, the muscle response is proportional to the integral of the product of the cortical stimulation sensitivity and the activating function. In the discretized form of the model, the TMS-evoked MEP amplitudes obtained from different stimulation locations (the elements of vector $\boldsymbol{m}$) are the product of the activating function

values and the motor representation area sensitivities or excitabilities (vector $\boldsymbol{x}$):

$$\boldsymbol{m} = \mathbf{E}'\boldsymbol{x}\,. \tag{2}$$

The ith row of $\mathbf{E}'$ contains the activating function of a TMS pulse used to evoke the corresponding motor response, i.e., the ith entry of $\boldsymbol{m}$.

The representation area sensitivities can be estimated by

$$\hat{\boldsymbol{x}} = \mathbf{E}'^{\dagger}\boldsymbol{m}\,. \tag{3}$$

$\mathbf{E}'^{\dagger}$, the pseudoinverse of $\mathbf{E}'$, can be calculated by applying the singular value decomposition:

$$\mathbf{E}' = \mathbf{U}\boldsymbol{\Sigma}\mathbf{V}^{\mathrm{T}}. \tag{4}$$

Then,

$$\hat{\boldsymbol{x}} = \mathbf{V}\boldsymbol{\Sigma}^{\dagger}\mathbf{U}^{\mathrm{T}}\boldsymbol{m}\,. \tag{5}$$

$\mathbf{V}$ and $\mathbf{U}$ are unitary matrices and $\boldsymbol{\Sigma}$ is a diagonal matrix containing the singular values of $\mathbf{E}'$. $\boldsymbol{\Sigma}^{\dagger}$ is calculated by replacing non-zero elements of $\boldsymbol{\Sigma}$ by their reciprocals and transposing the matrix. $\mathbf{U}^{\mathrm{T}}$ is the transpose of $\mathbf{U}$. The effect of noise (i.e., variability in the MEP responses) is reduced by regularization, e.g., by setting the smallest singular values in $\boldsymbol{\Sigma}$ to zero (Hämäläinen and Ilmoniemi 1994; Sarvas 1987). The appropriate level of regularization, however, is often challenging to determine objectively. We applied Wiener regularization (Numminen et al. 1995), where $\mathbf{E}'$ and $\boldsymbol{m}$ are orthonormalized to get $\mathbf{E}''$ and $\boldsymbol{m}'$, respectively; the estimate is then

$$\hat{\boldsymbol{x}} = \mathbf{E}''(\boldsymbol{h} \circ \boldsymbol{m}')\,, \tag{6}$$

where $\boldsymbol{h} \circ \boldsymbol{m}'$ means the Hadamard product, i.e., the element-wise multiplication, of $\boldsymbol{h}$ and $\boldsymbol{m}'$, where $\boldsymbol{h}$ is a vector of weighting factors h_i, which can be obtained from orthonormalized noise variances $\sigma^2_{\mathrm{n},i}$ and signal variance σ^2_{s}:

$$h_i = \frac{\sigma^2_{\mathrm{s}}}{\sigma^2_{\mathrm{s}} + \sigma^2_{\mathrm{n},i}}\,. \tag{7}$$

MEP amplitude variability was estimated by deriving it from a Gaussian distribution with the standard deviation being 74% of the motor responses' peak-to-peak amplitudes. The standard deviation was obtained from a previous study (Säisänen et al. 2008).

We calculated the nTMS-induced E-field distributions inside a spherically symmetric conductor by computing the mutual inductance between the nTMS coil model and the triangle construction (Ilmoniemi 2009) on a grid of points (with 1-mm spacing) placed on the cortical surface at the depth that was visualized during nTMS. The E-field was calculated for each stimulation location separately. Since the surface curvature of the head was not known, the origin of the sphere was at the center of each subject's head which was determined as the intersection of the imaginary lines going through the nasion and auricular points used in the navigation. Therefore, the parameters, e.g., the distance from the coil to the cortex and the distance from the coil to the center of the spherical head model, slightly varied. The coil model (figure-of-eight, inner diameter 34 mm, outer diameter 70 mm) consisted of ten turns of wire in both of its wings in one layer (Fig. 1), being a simplified model of the coil used in the experiments. The E-field profiles along the directions parallel and perpendicular to the maximum E-field direction matched the measured E-field profiles of the modeled coil (Nieminen et al. 2015). In every location on the grid, only the E-field component perpendicular to the nearest sulcus, which is the direction that activates the neurons most likely (Fox et al. 2004; Ilmoniemi et al. 1999), was considered. The perpendicular direction was approximated to coincide with the direction of the closest stimulation pulse, knowing that the pulses were directed perpendicular to the closest sulcus. Although the E-field calculations were conducted in a spherical head model applied at each stimulation location and the gyrification of the cortex or the tissue conductivities were not taken into account, the results were overlaid on individual magnetic resonance images (MRIs).

The MNE maps were calculated at discrete points using Eq. 6, and were then spline-interpolated (Borghetti et al. 2008; Julkunen 2014). The more conventional maps without E-field consideration were determined by applying only spline interpolation to the recorded MEP amplitudes. The areas and their CoGs as well as hotspots, i.e., the locations of maximum motor responses, were determined. The areas were outlined by thresholding, i.e., excluding all responses below a given amplitude. The thresholds were 10–90% of the maximum motor response. We tested the MNE method

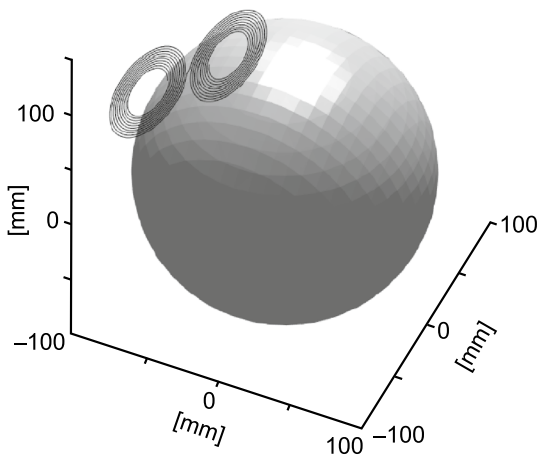

Fig. 1 The coil model (figure-of-eight, ten turns, inner diameter 34 mm, outer diameter 70 mm) used in the electric field calculations and the sphere with a 100-mm radius representing the head. The coil center was approximately 20 mm from the surface of the sphere

on simulated data in which the true representation areas in the brain were known for comparison. The method was also applied to estimate motor representations in healthy volunteers and in one chronic ischemic stroke patient. The same methods were used for the simulated and experimental data. Custom-made Matlab functions (R2015b, The MathWorks Inc., Natick, MA, USA) were utilized in the E-field calculations and data analysis.

Simulations

A cortical surface that would include the motor representation area was defined (Fig. 2, left column). One or two small regions were assumed to have a high sensitivity to E-field (areas with high magnitude in Fig. 2), whereas their surroundings were assumed to be insensitive (areas with zero magnitude in Fig. 2). The nTMS coil was approximately 30 mm above the grid, which was on average 90 mm from the center of the spherical conductivity model. The simulation included 90 different nTMS coil locations and orientations, which, as well as the coordinates of the motor representation area, were taken from previously recorded data in order to closely mimic experimental conditions. After computing the E-field distribution, we calculated the motor responses using Eq. 2 and the MNE map using Eq. 6. The mean values for the parameters M, μ, and σ from the healthy subjects were used in the sigmoidal function. The parameters were obtained by fitting a sigmoidal curve to the measured and averaged input–output data of each subject in the least-squares sense. Moreover, we performed a parametric study by simulating ten coil locations on a curved line above the motor representation area (Fig. 2f). Gaussian noise with zero mean and standard deviation of 74% of the motor response amplitudes was added to the responses. The noise was derived separately for each motor response, so that its standard deviation was proportional to the signal amplitude. The noise was used to model MEP variability. Other noise levels (with standard deviations of 25, 50, and 100% of the MEP amplitudes) were also tested for one simulation case in which the true representation area was identical to that in Fig. 2a. The simulations were conducted 1000 times, which was considered to be sufficient by checking that the means of the areas and CoGs had converged earlier to lie within the 95% confidence interval.

Experimental data

Six healthy right-handed volunteers (five males, age: 25–35 years) participated in the study. None of them had any contraindications for TMS or MRI; written informed consent was received from each of them. Structural T1 MRIs needed in the navigation were acquired with an Achieva 3.0T TX scanner (Philips, Eindhoven, The Netherlands). The stimulation was conducted with a Nexstim eXimia stimulator with a TMS-compatible electromyography (EMG) device, navigation software, a biphasic stimulator, and a figure-of-eight coil (version 3.2.2, Focal Bipulse, outer winding diameter ca. 70 mm, Nexstim Plc, Helsinki, Finland). EMG was measured from the first dorsal interosseous (FDI) muscle of the dominant hand. The mapping was started by searching for the optimal target, i.e., the location in which stimulation would induce the largest MEP amplitudes for FDI muscle, and measuring the resting motor threshold (rMT) in that location using the TMS Motor Threshold Assessment Tool 2.0 (Awiszus 2003; Awiszus and Borckardt 2012). Subsequent mappings were performed once with the stimulation intensity of 110% rMT and once with 120% rMT. The mapping began from the optimal target and extended to its surroundings until only MEPs lower than 50 μV in amplitude were evoked. The direction of the maximum of the induced E-field was perpendicular to the nearest sulcus. Only MEPs with amplitudes equal to or greater than 50 μV were accepted and MEPs induced after muscle tension were discarded. On another day, rMT was measured again and input–output curves were generated by applying stimuli at intensities of 90–150% of rMT in 10% steps while recording MEP amplitudes. Ten stimuli were given at each intensity. The slopes of input–output curves have been found to possess long-term stability in healthy subjects (Malcolm et al. 2006; Wolf et al. 2004); thus, the delay between the mapping and the input–output curve measurement was considered acceptable.

In addition, one 58-year-old male with chronic ischemic cortical stroke in the right hemisphere was studied 25 months after the incident. He had moderate recovery of the hand motor function. His head was scanned with a 1.5-T MRI device (Siemens Magnetom Avanto, Siemens Healthcare, Erlangen, Germany). His both hemispheres were stimulated with a biphasic Nexstim eXimia stimulator using a figure-of-eight coil (version 3.2.2, Focal Bipulse, outer winding diameter ca. 70 mm) while EMG was measured from the contralateral extensor digitorum communis and abductor pollicis brevis muscles. The rMT was determined for both muscles as the minimum stimulator output evoking MEPs of minimum 50 μV in amplitude in a resting muscle, in at least five out of ten given stimuli (Rothwell et al. 1999). The muscles were mapped separately at 110% of rMT, and the direction of the maximum of the E-field was kept mostly perpendicular to the nearest sulcus.

The MNE calculations were conducted as explained above. The sigmoidal function (Eq. 1) was fitted in the least-squares sense to the averaged input–output data of each healthy subject to obtain M, μ, and σ. For the patient, the input–output data were not measured. Instead, the mean sigmoidal parameters obtained from

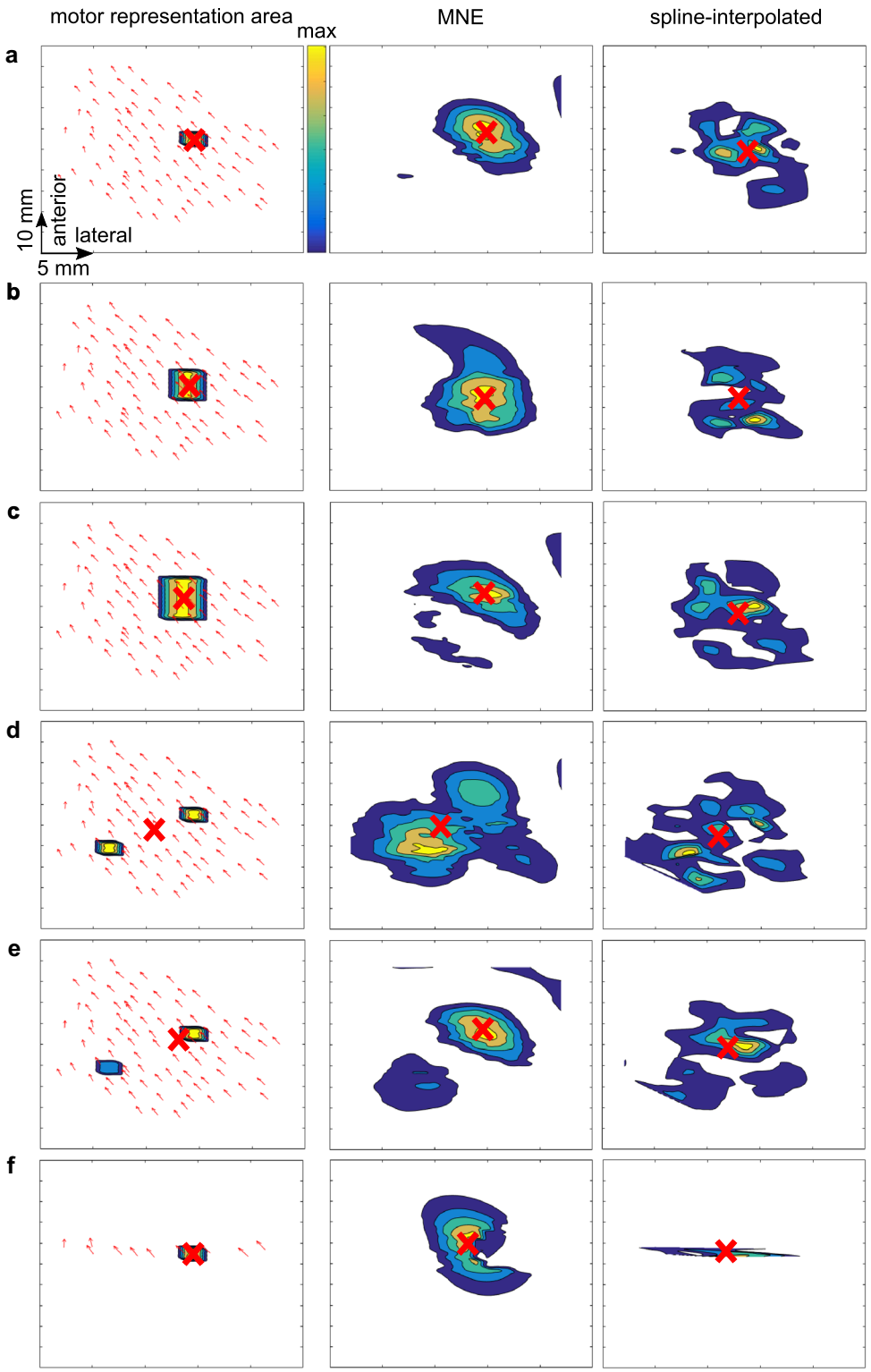

Fig. 2 Examples of six different simulations (a–f). *Left column*: the simulated motor representation areas with small *red arrows* illustrating the locations and orientations of the stimulation targets on the cortex. *Center column*: the maps calculated from noisy data using minimum-norm estimation (noise 74% of response magnitude). *Right column*: the spline-interpolated maps. **a** A small simulated representation area. **b** A medium-sized simulated representation area. **c** A large simulated representation area. **d** Two equal-sized simulated representation areas with equal sensitivities. **e** Two simulated representation areas with different sensitivities. **f** A small simulated representation area with ten stimulation target locations on a line over the presumed motor area. The axes are oriented similarly in each map and the contour lines are drawn at ten (*dark blue*), 30, 50, 70, and 90% (*yellow*) of the maximum value of response amplitude in each map. The centers of gravity of the data thresholded at 50% are shown as large *red crosses*. *MNE* minimum-norm estimation. (Color figure online)

the healthy subjects were used to define the patient's sigmoidal function. The recorded locations and orientations of the coil were used in the E-field calculations. The distance from the coil center to the modeled cortical surface was approximately 20 mm. The rMTs were: 38±10% (mean ± standard deviation) (healthy), 34±2% (stroke, unaffected hemisphere), and 46±5% (stroke, affected hemisphere) of the maximum stimulator output.

Results

Simulations

The MNE method accurately located the activation site from the simulated noiseless data; the Euclidean distance between the CoGs of the estimate and the simulated representation area was 0.6 mm, whereas between the more conventional spline-interpolated CoG and the simulated CoG the distance was 3.3 mm. The areas were 1.7 cm^2 (MNE map) and 0.7 cm^2 (spline-interpolated map) for the data without noise, whereas the simulated area was 0.1 cm^2. As the noise level increased, the estimation became less accurate and the role of regularization became more important. The means and standard deviations of Euclidean distances between the simulated and estimated CoGs were greater with increasing noise levels. The distance of the MNE CoG from the simulated CoG increased to 0.8, 1.1, 1.4, and 1.7 mm when the standard deviation of the noise was increased to 25, 50, 74, and 100% of the MEP amplitudes, respectively. For a more conventional spline-interpolated map, the CoG distance increased to 3.5, 3.6, 3.8, and 3.9 mm, respectively. The MNE map became 18% broader and the spline-interpolated area diminished by 43% when the standard deviation of the noise was 100% of the MEP amplitudes compared to the noiseless data. The MNE map of the noisy data occasionally had additional local hotspots scattered around the correct location. Appropriate thresholding seems to reduce the effect of noise, allowing one to obtain a more robust estimate of the motor representation area.

The results of the simulations at noise level of 74% are shown in Table 1 and in Fig. 2. The average Euclidean distance from the MNE CoG to simulated CoG was shorter than the average Euclidean distance between the spline-interpolated and simulated CoG and the areas of the 50% thresholded maps were larger for MNE than for spline-interpolated maps. The more conventional 50-μV thresholding in spline-interpolated maps resulted in much larger areas. For example, the simulation presented in Fig. 2a resulted in an area of 7.3 cm^2 (range: 6.3–8.0 cm^2) when thresholded at 50 μV. When the simulated area was enlarged (Fig. 2b–c), the Euclidean distances and the areas were almost the same as previously (Table 1). When the simulated representation area consisted of two distinct regions (Fig. 2d–e), the differences between the simulated and MNE CoGs increased. Figure 2f shows the results of the line-mapping simulation. Even in this simulation, the MNE was able to estimate the representation area well, whereas the spline interpolation resulted in a narrow map in the anterior–posterior direction but a wide map in the medial–lateral direction.

Experimental Data

Figures 3 and 4 present the experimental data from the healthy subjects. The CoGs and hotspots were located quite similarly in the MNE and spline-interpolated maps (Euclidean distances: CoGs 6.7 ± 4.3 mm, hotspots 8.9 ± 7.2 mm). The areas of the maps differed; when pooling all the mappings of the healthy subjects with 10, 50, and 90% thresholding levels, the MNE map was on average 216% larger than the spline-interpolated map when they were thresholded at the same percentage levels (MNE area ranging from 0.2 to 18.5 times the spline-interpolated area). Figure 5 shows the spline-interpolated and MNE maps of the stroke patient. In the patient data, the Euclidean distance of the CoGs was on average 4.4 ± 1.9 mm and the hotspots were separated by 6.1 ± 1.9 mm. On average, the MNE map was 391% larger than the spline-interpolated map (MNE area being 0.7–11.9 times the spline-interpolated area). Again, the 50-μV thresholding resulted in larger areas than the percentage thresholding in the healthy subjects and in the patient.

Table 1 The results of the simulations presented in Fig. 2

	Simulated	Minimum-norm estimate		Spline-interpolated	
	Area (cm^2)	Area [cm^2] [mean (range)]	Distance [mm] (mean ± standard deviation)	Area [cm^2] [mean (range)]	Distance [mm] (mean ± standard deviation)
Figure 2a	0.1	1.8 (1.1–3.8)	1.4 ± 0.8	0.4 (0.1–1.8)	3.8 ± 1.4
Figure 2b	0.2	1.8 (1.8–2.0)	1.5 ± 0.1	0.5 (0.4–0.8)	4.1 ± 0.1
Figure 2c	0.5	1.9 (1.2–3.8)	1.4 ± 0.8	0.5 (0.1–1.7)	3.9 ± 1.4
Figure 2d	0.2	2.6 (1.4–4.6)	2.4 ± 1.4	0.6 (0.1–1.6)	3.9 ± 2.1
Figure 2e	0.2	2.2 (2.1–2.7)	1.8 ± 0.1	0.5 (0.5–0.7)	3.1 ± 0.1
Figure 2f	0.1	1.4 (1.2–1.5)	4.2 ± 1.3	0.1 (0.0–0.1)	5.6 ± 1.7

The simulated area is the area which is estimated. The areas are reported for the 50%-thresholded data and the distances are Euclidean distances between the simulated center of gravity (CoG) and either the minimum-norm estimate CoG or spline-interpolated CoG of the 50%-thresholded data. The standard deviation of the Gaussian noise is 74% of response magnitude

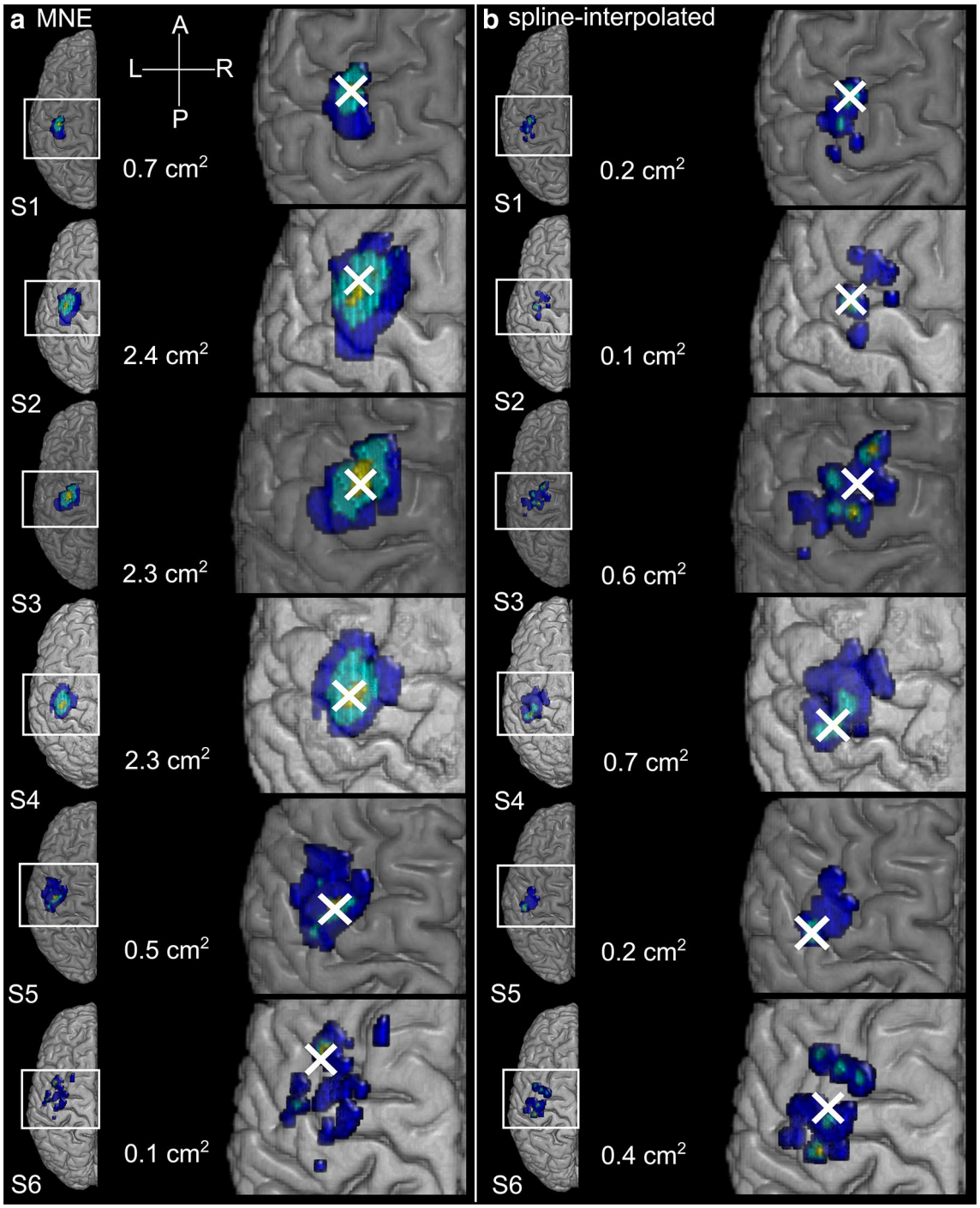

Fig. 3 The maps and the centers of gravity (*white crosses*) of FDI muscle of healthy subjects on individual MRIs. The stimulation intensity was 110% rMT. The maps are thresholded at 10 (*dark blue*), 50 (*cyan*), and 90% (*yellow*) of the MEP amplitude maximum. The centers of gravity and the area values are for the 50%-thresholded data. Only the mapped hemispheres are shown. **a** MNE and **b** spline-interpolated maps (without electric field consideration). *A* anterior, *FDI* first dorsal interosseous, *L* left, *MEP* motor-evoked potential, *MNE* minimum-norm estimation, *MRI* magnetic resonance imaging, *P* posterior, *R* right, *rMT* resting motor threshold, *S* subject. (Color figure online)

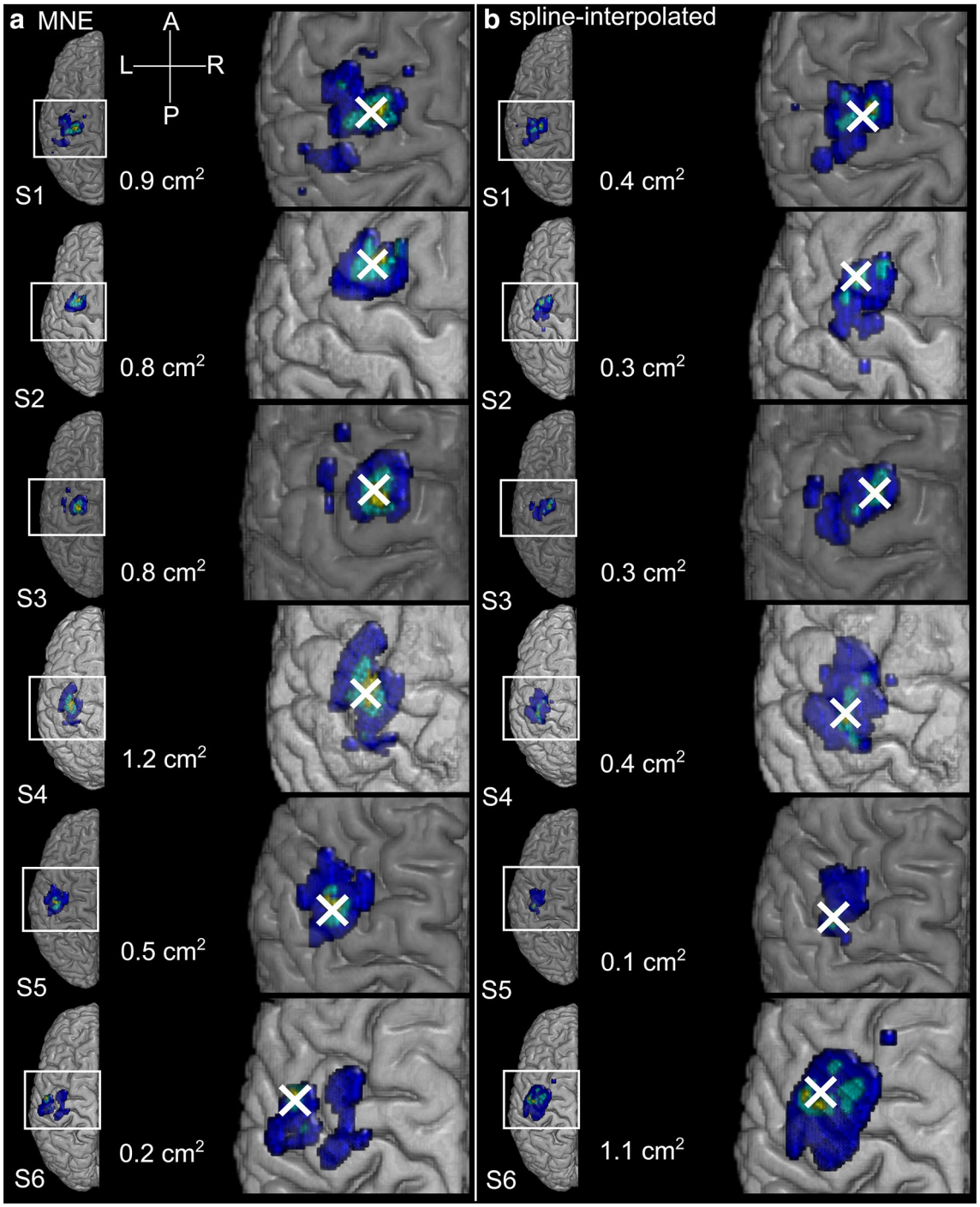

Fig. 4 The maps and the centers of gravity (*white crosses*) of FDI muscle of healthy subjects on individual MRIs. The stimulation intensity was 120% rMT. The maps are thresholded at 10 (*dark blue*), 50 (*cyan*), and 90% (*yellow*) of the MEP amplitude maximum. The centers of gravity and the area values are for the 50%-thresholded data. Only the mapped hemispheres are shown. **a** MNE and **b** spline-interpolated maps (without electric field consideration). *A* anterior, *FDI* first dorsal interosseous, *L* left, *MEP* motor-evoked potential, *MNE* minimum-norm estimation, *MRI* magnetic resonance imaging, *P* posterior, *R* right, *rMT* resting motor threshold, *S* subject. (Color figure online)

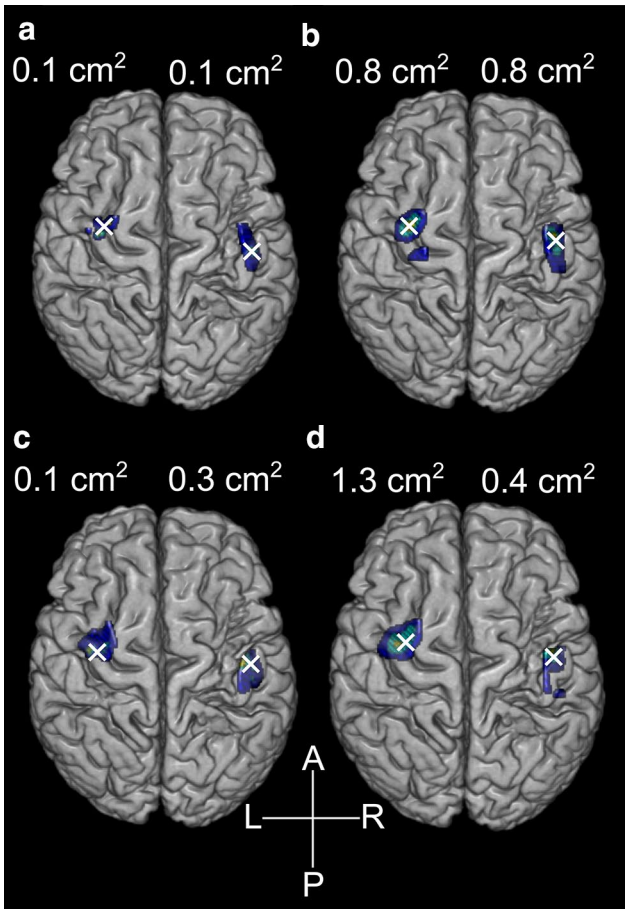

Fig. 5 The maps and the centers of gravity (*white crosses*) of the stroke patient. The maps are thresholded at 10 (*dark blue*), 50 (*cyan*), and 90% (*yellow*) of the MEP amplitude maximum. The centers of gravity and area values are for the 50%-thresholded data. **a** Spline-interpolated map of abductor pollicis brevis (APB) without electric field consideration. **b** MNE of APB. **c** Spline-interpolated map of extensor digitorum communis (EDC) without electric field consideration. **d** MNE of EDC. *A* anterior, *L* left, *MEP* motor-evoked potential, *MNE* minimum-norm estimation, *P* posterior, *R* right. (Color figure online)

Discussion

We developed an nTMS–MNE method for estimating primary motor representation areas, taking into account the E-field distribution that tends to blur conventional nTMS motor maps. Our method was able to locate the activation site from the simulated data. However, as the true activation areas in the experimental data were unknown, we can only speculate about the accuracy when interpreting measured data. When compared with the spline-interpolated maps, the CoG and hotspot locations were close but on average the MNE maps were larger than the more conventional spline-interpolated ones when thresholded at the same percentage level (10, 50, or 90% of maximum). The difference might be due to the regularization which blurs the MNE maps while reducing the effect of noise.

The MNE maps are in different units than the conventional MEP response maps. Commonly, the MEP areas are outlined with a 50-μV contour, as that usually is the minimum amplitude for acceptable resting MEPs (Jussen et al. 2016; Rossini et al. 2015), but in this study, both maps were thresholded at different percentage levels in order to compare them better. If the outline of the map is required, thresholding is necessary due to the large number of small values at the edges of the maps. This thresholding influences the area of the estimates; hence, its use should be carefully contemplated. Based on our simulations, the 50% threshold seems to estimate the location and the area of the motor representations quite robustly. If spline-interpolated maps without the E-field consideration were thresholded at a level based on the percentage of the maximum value, they might be more accurate than conventional 50-μV maps, which were larger. The small motor responses when stimulating at the edges of the nTMS maps might be induced because the broad E-field likely stimulates the center of the map in addition to the actual stimulation target location. MNE estimates only the primary area of excitation by considering the E-field-distribution-induced spreading, which is conventionally seen in motor maps. The areas outside the MNE map can, therefore, produce motor responses when the maximum E-field is targeted there.

The MNE method was tested on simulated data for which the true representation areas were known. One step was the simulation with ten stimulation locations on a curved line. Usually in healthy subjects, the primary motor area is located in the pre-central gyrus and a line-mapping along the gyrus could already give information about the motor representation. This kind of mapping, however, is only used in basic nTMS research, for example, to reveal the mediolateral differences in cortical muscle representations (Raffin et al. 2015). Based on our simulations, MNE could locate the primary motor area even in this case. However, the resolution in the direction perpendicular to the gyrus was poor, as the mapping did not provide sufficient information in that direction. On the other hand, the spline-interpolated map had poor resolution in the direction parallel to the gyrus. This implies that fewer stimulation points might be needed for the MNE method than for the method without E-field consideration to estimate the motor representation. However, more stimulation points make the estimate more accurate. Based on the simulations, the MNE method is able to estimate the motor representation areas, possibly even with less stimulation pulses than needed for conventional methods.

Conventional MEP mapping and the input–output curves may be sensitive to MEP variability and outliers. We reduced the effect of outliers by averaging MEP amplitudes

in the input–output data and by fitting a sigmoidal curve to the values. Furthermore, the MEPs occurring after muscle tension were rejected from the analysis to reduce the number of outliers. However, based on the simulations with different noise levels, the MNE method seems to be sensitive also to the variability of the MEPs. Regularization might reduce this influence. Moreover, MEP outliers may dominate even after averaging. MEP variability distribution is dependent on the stimulation intensity, and if this behavior is taken into account in the future, the input–output data analysis could be improved (Goetz et al. 2014).

Previously, Bohning et al. (2001) applied an approach similar to the introduced MNE method to determine the cortical area activated by TMS. They measured the magnitude of the E-field in a spherical phantom and computed the deconvolution of the TMS maps and the E-field. Contrary to their study, we calculated the E-field in a spherical head model and considered also the direction of the E-field.

Limitations

Since MEPs are non-linearly related to the stimulation intensity, and since MNE is a linear transformation, the non-linearity of the responses was taken into account by transforming the induced E-field by a sigmoidal function in order to obtain an activating function that would be approximately proportional to MEPs; this transformation was assumed to be the same for all cortical locations. This assumption may have influenced the results because, in reality, the sigmoidal function may vary by location. Input–output data were not measured from the stroke patient and the use of the mean input–output parameters of healthy subjects might have distorted the results. In addition, least-squares fitting of input–output data in the linear domain might not be the optimal method due to MEP distribution characteristics (Goetz et al. 2014).

The E-field values were calculated in the spherical head model instead of a realistic model, in which the computations could be carried out, e.g., by the boundary element method. The E-field distribution is affected by the conductivity geometry of the head (Ilmoniemi et al. 1999); therefore, a realistic head model would be more accurate than the spherical model. In addition, estimated stimulation areas have been larger for the spherical model than for a realistic model (Opitz et al. 2014) and therefore, the use of a realistic model could lead to smaller motor maps than shown in this study. We did not take the gyrification of the cortex into account which may have reduced the spatial specificity of our estimation (Opitz et al. 2014) and potentially lead to deviations from the actual representation areas. Furthermore, the E-field calculations may have been affected by the stroke lesion in the patient. The locally-fitted spherical model is, however, easier to implement and is considered sufficient for the motor cortex (Nummenmaa et al. 2013). In the spherical model, the nTMS-induced E-field is also straightforward to measure (Nieminen et al. 2015). In addition, we calculated the motor maps only using the E-field component perpendicular to the closest sulcus. In a preliminary investigation, we conducted a similar analysis using the norm of the E-field but it resulted in less accurate results. The coil model might in principle also have affected the results, as we used a simplified figure-of-eight coil model to reduce the computational load in the calculations.

Moreover, the regularization affects the estimates. We used Wiener regularization (Numminen et al. 1995), for which information about the noise amplitude should be known or approximated because optimal regularization depends on the signal-to-noise ratio. However, there is no consensus on the best regularization method or on how the noise level should be determined.

In the future, the correct motor representation location and the amount of thresholding should be validated by DCS mappings. DCS mapping could also reveal if our model was biased, i.e., whether it is better suited for the simulated than for the experimental data. Limitations regarding regularization should be reduced and different regularization methods should be compared with each other. If these issues can be overcome, the MNE method could provide a useful way of analyzing nTMS mappings in healthy subjects and, for example, in stroke patients.

In conclusion, we applied MNE to estimate nTMS motor maps. The MNE method could be more advantageous than the conventional methods if it can be shown to provide results that are similar to those obtained with DCS.

Acknowledgements The study was funded by the State Research Funding (Research Committee of the Kuopio University Hospital Catchment Area, projects 5041730 and 5041747, Kuopio, Finland); Finnish Cultural Foundation, Helsinki, Finland; Cancer Society of Finland, Helsinki, Finland; Päivikki and Sakari Sohlberg Foundation, Helsinki, Finland; Academy of Finland (Decisions Nos. 255347, 265680, and 294625), Helsinki, Finland; Russian Academic Excellence Project '5-100', RFBR Grant (No. 16-04-01883) and Skolkovo personal grant "Umnik". The funding sources had no involvement in the study design, in the collection, analysis and interpretation of data, in the writing of the report, or in the decision to submit the article for publication.

Compliance with Ethical Standards

Conflict of interest Petro Julkunen and Jaakko O. Nieminen have received unrelated consulting fees from Nexstim Plc, Elisa Kallioniemi has received unrelated travel support from Nexstim Plc, and Risto J. Ilmoniemi is an advisor and a minority shareholder of the company. The other authors declare no conflict of interest.

Ethical Approval All procedures performed in studies involving human participants were in accordance with the ethical standards of the institutional and/or national research committee and with the 1964

Helsinki Declaration and its later amendments or comparable ethical standards.

Informed Consent Informed consent was obtained from all individual participants included in the study.

References

Awiszus F (2003) TMS and threshold hunting. Suppl to Clin Neurophysioly 56:13–23

Awiszus F, Borckardt JJ (2012) TMS Motor Threshold Assessment Tool 2.0 http://clinicalresearcher.org/software.htm. Accessed 2 June 2014

Bohning DE, He L, George MS, Epstein CM (2001) Deconvolution of transcranial magnetic stimulation (TMS) maps. J Neural Transm 108:35–52

Borghetti D, Sartucci F, Petacchi E, Guzzetta A, Piras MF, Murri L, Cioni G (2008) Transcranial magnetic stimulation mapping: a model based on spline interpolation. Brain Res Bull 77:143–148

Bungert A, Antunes A, Espenhahn S, Thielscher A (2016) Where does TMS stimulate the motor cortex? Combining electrophysiological measurements and realistic field estimates to reveal the affected cortex position. Cereb Cortex 1–12

Danner N, Julkunen P, Könönen M, Säisänen L, Nurkkala J, Karhu J (2008) Navigated transcranial magnetic stimulation and computed electric field strength reduce stimulator-dependent differences in the motor threshold. J Neurosci Methods 174:116–122

Devanne H, Lavoie BA, Capaday C (1997) Input-output properties and gain changes in the human corticospinal pathway. Exp Brain Res 114:329–338

Fox PT, Narayana S, Tandon N, Sandoval H, Fox SP, Kochunov P, Lancaster JL (2004) Column-based model of electric field excitation of cerebral cortex. Hum Brain Mapp 22:1–14

Goetz SM, Luber B, Lisanby SH, Peterchev AV (2014) A novel model incorporating two variability sources for describing motor evoked potentials. Brain Stimul 7:541–552

Hämäläinen MS, Ilmoniemi RJ (1994) Interpreting magnetic fields of the brain: minimum norm estimates. Med Biol Eng Comput 32:35–42

Heald A, Bates D, Cartlidge NEF, French JM, Miller S (1993) Longitudinal study of central motor conduction time following stroke: 2. Central motor conduction measured within 72 h after stroke as a predictor of functional outcome at 12 months. Brain 116:1371–1385

Ilmoniemi RJ (2009) The triangle phantom in magnetoencephalography. J Jpn Biomagn Bioelectromagn Soc 22:44–45

Ilmoniemi RJ, Ruohonen J, Karhu J (1999) Transcranial magnetic stimulation—a new tool for functional imaging of the brain. Crit Rev Biomed Eng 27:241–284

Jang SH, Ahn SH, Sakong J, Byun WM, Choi BY, Chang CH, Bai D, Son SM (2010) Comparison of TMS and DTT for predicting motor outcome in intracerebral hemorrhage. J Neurol Sci 290:107–111

Julkunen P (2014) Methods for estimating cortical motor representation size and location in navigated transcranial magnetic stimulation. J Neurosci Methods 232:125–133

Julkunen P, Säisänen L, Danner N, Awiszus F, Könönen M (2012) Within-subject effect of coil-to-cortex distance on cortical electric field threshold and motor evoked potentials in transcranial magnetic stimulation. J Neurosci Methods 206:158–164

Jussen D, Zdunczyk A, Schmidt S, Rösler J, Buchert R, Julkunen P, Karhu J, Brandt S, Picht T, Vajkoczy P (2016) Motor plasticity after extra-intracranial bypass surgery in occlusive cerebrovascular disease. Neurology 87:27–35

Kallioniemi E, Julkunen P (2016) Alternative stimulation intensities for mapping cortical motor area with navigated TMS. Brain Topogr 29:395–404

Kallioniemi E, Pitkänen M, Säisänen L, Julkunen P (2015) Onset latency of motor evoked potentials in motor cortical mapping with neuronavigated transcranial magnetic stimulation. Open Neurol J 9:62–69

Liepert J, Bauder H, Miltner WHR, Taub E, Weiller C (2000) Treatment-induced cortical reorganization after stroke in humans. Stroke 31:1210–1216

Malcolm MP, Triggs WJ, Light KE, Shechtman O, Khandekar G, Gonzalez Rothi LJ (2006) Reliability of motor cortex transcranial magnetic stimulation in four muscle representations. Clin Neurophysiol 117:1037–1046

Matthäus L, Trillenberg P, Fadini T, Finke M, Schweikard A (2008) Brain mapping with transcranial magnetic stimulation using a refined correlation ratio and Kendall's τ. Stat Med 27:5252–5270

Nieminen JO, Koponen LM, Ilmoniemi RJ (2015) Experimental characterization of the electric field distribution induced by TMS devices. Brain Stimul 8:582–589

Nummenmaa A, Stenroos M, Ilmoniemi RJ, Okada YC, Hämäläinen MS, Raij T (2013) Comparison of spherical and realistically shaped boundary element head models for transcranial magnetic stimulation navigation. Clin Neurophysiol 124:1995–2007

Numminen J, Ahlfors S, Ilmoniemi R, Montonen J, Nenonen J (1995) Transformation of multichannel magnetocardiographic signals to standard grid form. IEEE Trans Biomed Eng 42:72–78

Opitz A, Legon W, Rowlands A, Bickel WK, Paulus W, Tyler WJ (2013) Physiological observations validate finite element models for estimating subject-specific electric field distributions induced by transcranial magnetic stimulation of the human motor cortex. NeuroImage 81:253–264

Opitz A, Zafar N, Bockermann V, Rohde V, Paulus W (2014) Validating computationally predicted TMS stimulation areas using direct electrical stimulation in patients with brain tumors near precentral regions. NeuroImage 4:500–507

Paiva WS, Fonoff ET, Marcolin MA, Cabrera HN, Teixeira MJ (2012) Cortical mapping with navigated transcranial magnetic stimulation in low-grade glioma surgery. Neuropsychiatr Dis Treat 8:197–201

Parker RL (1977) Understanding inverse theory. Annu Rev Earth Planet Sci 5:35–64

Picht T, Schmidt S, Brandt S, Frey D, Hannula H, Neuvonen T, Karhu J, Vajkoczy P, Suess O (2011) Preoperative functional mapping for rolandic brain tumor surgery: comparison of navigated transcranial magnetic stimulation to direct cortical stimulation. Neurosurgery 69:581–589

Picht T, Krieg SM, Sollmann N, Rösler J, Niraula B, Neuvonen T, Savolainen P, Lioumis P, Mäkelä JP, Deletis V, Meyer B, Vajkoczy P, Ringel F (2013) A comparison of language mapping by preoperative navigated transcranial magnetic stimulation and direct cortical stimulation during awake surgery. Neurosurgery 72:808–819

Pitkänen M, Kallioniemi E, Julkunen P (2015) Extent and location of the excitatory and inhibitory cortical hand representation maps: a navigated transcranial magnetic stimulation study. Brain Topogr 28:657–665

Raffin E, Pellegrino G, Di Lazzaro V, Thielscher A, Siebner HR (2015) Bringing transcranial mapping into shape: sulcus-aligned mapping captures motor somatotopy in human primary motor hand area. NeuroImage 120:164–175

Rossini PM, Burke D, Chen R, Cohen LG, Daskalakis Z, Di Iorio R, Di Lazzaro V, Ferreri F, Fitzgerald PB, George MS, Hallett M, Lefaucheur JP, Langguth B, Matsumoto H, Miniussi C, Nitsche

MA, Pascual-Leone A, Paulus W, Rossi S et al (2015) Non-invasive electrical and magnetic stimulation of the brain, spinal cord, roots and peripheral nerves: basic principles and procedures for routine clinical and research application. An updated report from an I.F.C.N. Committee. Clin Neurophysiol 126:1071–1107

Rothwell JC, Hallett M, Berardelli A, Eisen A, Rossini P, Paulus W (1999) Magnetic stimulation: motor evoked potentials. Electroencephalogr Clin Neurophysiol Suppl 52:97–103

Säisänen L, Julkunen P, Niskanen E, Danner N, Hukkanen T, Lohioja T, Nurkkala J, Mervaala E, Karhu J, Könönen M (2008) Motor potentials evoked by navigated transcranial magnetic stimulation in healthy subjects. J Clin Neurophysiol 25:367–372

Sarvas J (1987) Basic mathematical and electromagnetic concepts of the biomagnetic inverse problem. Phys Med Biol 32:11–22

Thickbroom GW, Sammut R, Mastaglia FL (1998) Magnetic stimulation mapping of motor cortex: factors contributing to map area. Electroencephalogr Clin Neurophysiol 109:79–84

Thielscher A, Kammer T (2002) Linking physics with physiology in TMS: a sphere field model to determine the cortical stimulation site in TMS. NeuroImage 17:1117–1130

Thielscher A, Wichmann FA (2009) Determining the cortical target of transcranial magnetic stimulation. NeuroImage 47:1319–1330

Traversa R, Cicinelli P, Bassi A, Rossini PM, Bernardi G (1997) Mapping of motor cortical reorganization after stroke: a brain simulation study with focal magnetic pulses. Stroke 28:110–117

Vitikainen A-M, Salli E, Lioumis P, Mäkelä JP, Metsähonkala L (2013) Applicability of nTMS in locating the motor cortical representation areas in patients with epilepsy. Acta Neurochir 155:507–518

Wassermann EM, McShane LM, Hallett M, Cohen LG (1992) Noninvasive mapping of muscle representations in human motor cortex. Electroencephalogr Clin Neurophysiol 85:1–8

Wassermann EM, Pascual-Leone A, Valls-Solé J, Toro C, Cohen LG, Hallett M (1993) Topography of the inhibitory and excitatory responses to transcranial magnetic stimulation in a hand muscle. Electroencephalogr Clin Neurophysiol 89:424–433

Wilson SA, Thickbroom GW, Mastaglia FL (1993) Topography of excitatory and inhibitory muscle responses evoked by transcranial magnetic stimulation in the human motor cortex. Neurosci Lett 154:52–56

Wolf SL, Butler AJ, Campana GI, Parris TA, Struys DM, Weinstein SR, Weiss P (2004) Intra-subject reliability of parameters contributing to maps generated by transcranial magnetic stimulation in able-bodied adults. Clin Neurophysiol 115:1740–1747